Synthesis of 4-hydroxyindole fused isocoumarin derivatives and their fluorescence "Turn-off" sensing of Cu(II) and Fe(III) ions

Sudipta Pathak, Doyel Das, Ashis Kundu, Subhendu Maity, Nikhil Guchhait and Animesh Pramanik*

Department of Chemistry, University of Calcutta, 92, A. P. C. Road, Kolkata-700 009, India
E-mail: animesh_in2001@yahoo.co.in

Supporting Information

Contents   Pages

Photophysical Study

Spectroscopic grade solvents were purchased from Spectrochem, India and used without further distillation. The concentration of the ligands was maintained at 5×10^{-5} M. Absorption and emission measurements were performed using Hitachi UV-vis U-3501 spectrophotometer and Perkin Elmer LS-55 fluorimeter respectively. The backgrounds of the recorded spectra were appropriately subtracted with a blank solvent in order to eliminate any spectral interference. The experiments have been carried out at room temperature.

Theoretical calculations have been performed using Gaussian 09 suite of program. Optimization of the ground state geometry has been carried out at DFT level using B3LYP hybrid functional and 6-31+G(d,p) basis set. The excited state was regenerated by the vertical excitation of the optimized ground state geometry followed by optimization at the excited state using TDDFT method and B3LYP/6-31+G(d,p) functional and basis set.

Fluorescence quantum yields (Φ_F) in various solvents are determined using the following equation[1]

$$\Phi_{sample} = [(A_{std}\, F_{sample}\, \eta^2_{sample} / A_{sample}\, F_{std}\, \eta^2_{std})]\, \Phi_{std}$$

In this equation Φ_{sample} and Φ_{std} are the quantum yields of sample and standard, respectively; A_{std} and A_{sample} are the absorbance of the sample and standard, respectively; F_{sample} and F_{std} are integrated emission area across the fluorescence band and η_{sample} and η_{std} are the refractive indexes of the sample and standard solution, respectively.

Table S1. Spectroscopic data of **9** in three solvents

Compounds	Solvent	λ_{abs}(nm)	λ_{em}(nm)	Φ_F [a]

9a	CH$_2$Cl$_2$	382	496	0.42
	CH$_3$CN	385	501	0.47
	CH$_3$OH	395	511	0.23
9b	CH$_2$Cl$_2$	378	494	0.42
	CH$_3$CN	382	499	0.58
	CH$_3$OH	391	509	0.28
9c	CH$_2$Cl$_2$	382	496	0.67
	CH$_3$CN	381	500	0.54
	CH$_3$OH	391	510	0.30
9d	CH$_2$Cl$_2$	376	492	0.64
	CH$_3$CN	380	502	0.68
	CH$_3$OH	391	511	0.30
9e	CH$_2$Cl$_2$	377	496	0.66
	CH$_3$CN	377	501	0.65
	CH$_3$OH	391	509	0.35
9f	CH$_2$Cl$_2$	381	496	0.53
	CH$_3$CN	380	499	0.57

	CH₃OH	389	511	0.31

Table S2. Absorbance (A), fluorescence emission area (F) and refractive index (η) of **9** in different Solvents

Product	Solvent	Absorbance (A)	Emission area (F)	Refractive index (η)
9a	CH₃CN	0.172	59521	1.3460
	CH₂Cl₂	0.105	33140	1.4242
	MeOH	0.105	17695	1.3314
9b	CH₃CN	0.095	40667	1.3460
	CH₂Cl₂	0.110	34254	1.4242
	MeOH	0.093	19166	1.3314
9c	CH₃CN	0.128	51617	1.3460
	CH₂Cl₂	0.097	46373	1.4242
	MeOH	0.112	24971	1.3314
9d	CH₃CN	0.081	41037	1.3460
	CH₂Cl₂	0.092	43734	1.4242
	MeOH	0.091	20594	1.3314
9e	CH₃CN	0.125	60388	1.3460
	CH₂Cl₂	0.091	44923	1.4242
	MeOH	0.081	21298	1.3314
9f	CH₃CN	0.134	56876	1.3460
	CH₂Cl₂	0.146	58046	1.4242
	MeOH	0.098	22459	1.3314

Related reference.

(1) D. F. Eaton, *Pure & Appl. Chem.* **1988**, *60* (7), 1107.
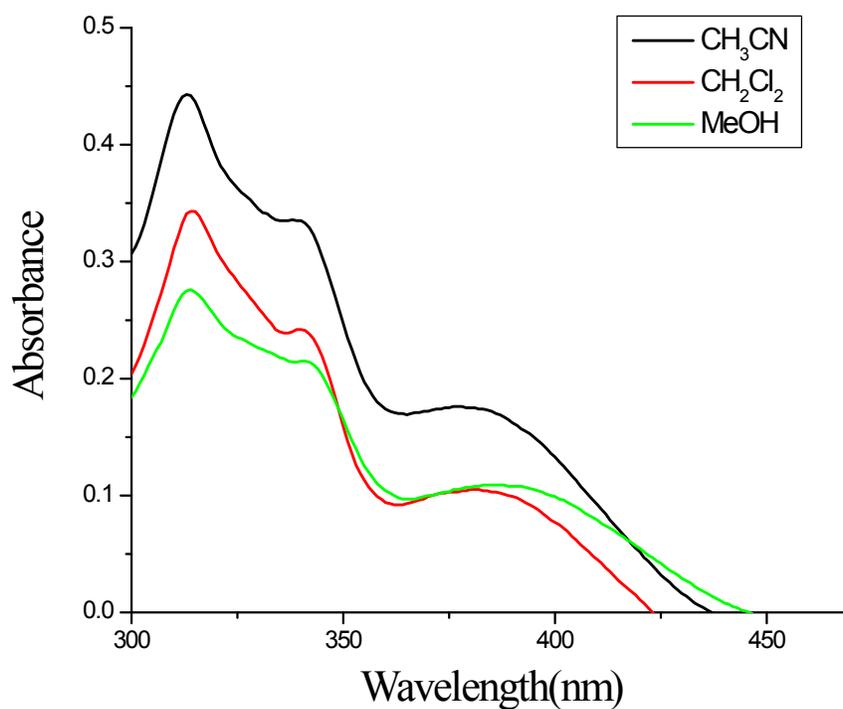
Fig. S1 UV-vis absorption spectra of compound **9a** in different solvents ([**9a**] = ~2×10^{-5} M).
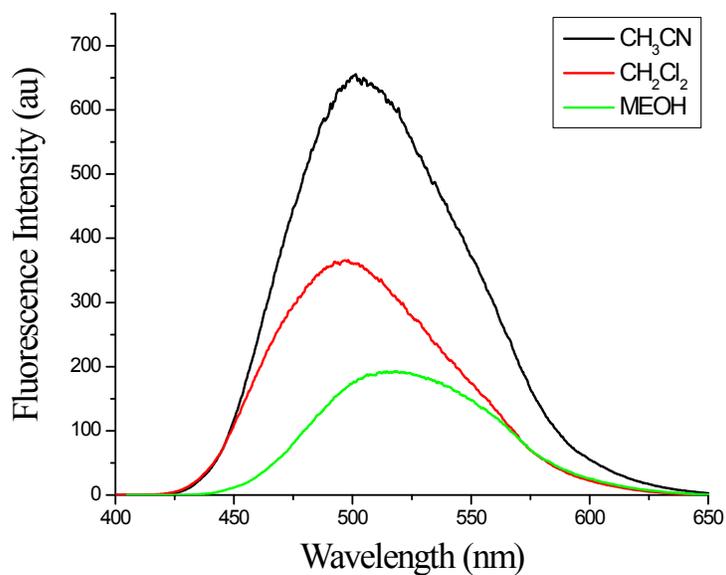
Fig. S2. Fluorescence emission spectra of **9a** in different solvents ([**9a**] = ~2×10^{-5} M).
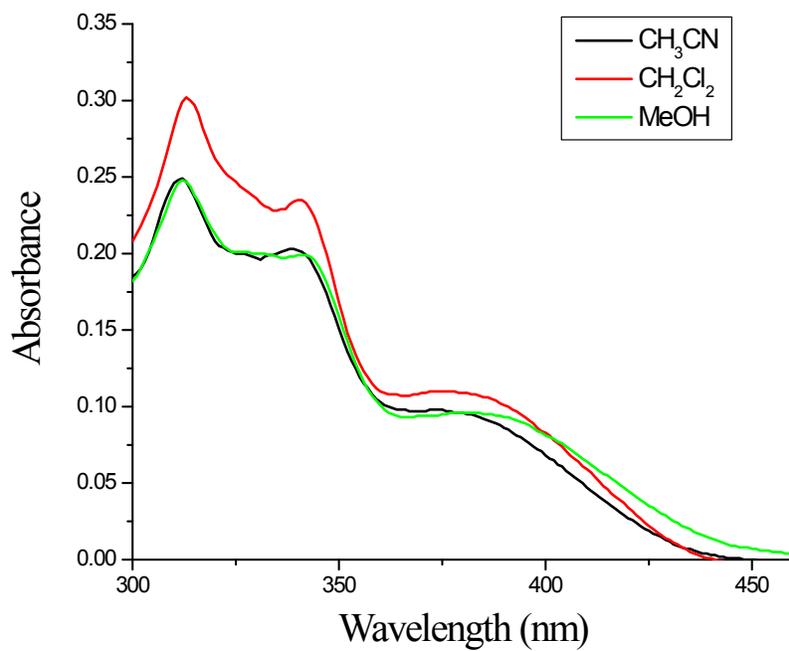
Fig. S3 UV-vis absorption spectra of compound **9b** in different solvents ([**9b**] = ~2×10^{-5} M).
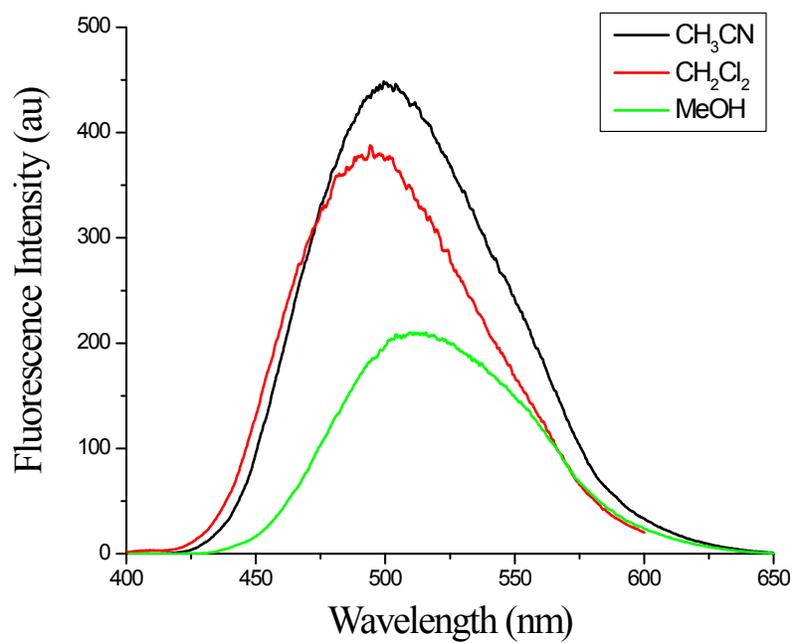
Fig. S4 Fluorescence emission spectra of **9b** in different solvents ([**9b**] = ~2×10^{-5} M).
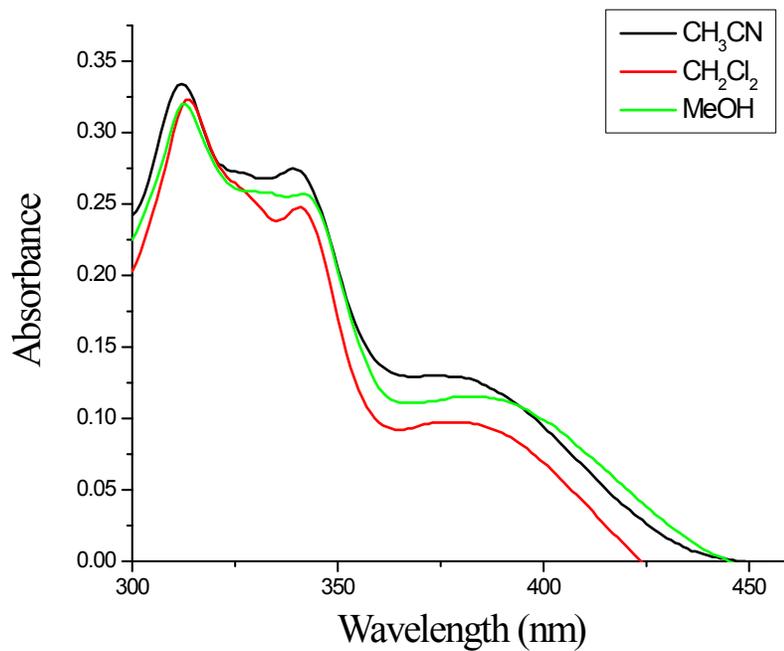
Fig. S5 UV-vis absorption spectra of compound **9c** in different solvents ([**9c**] = ~2×10^{-5} M).
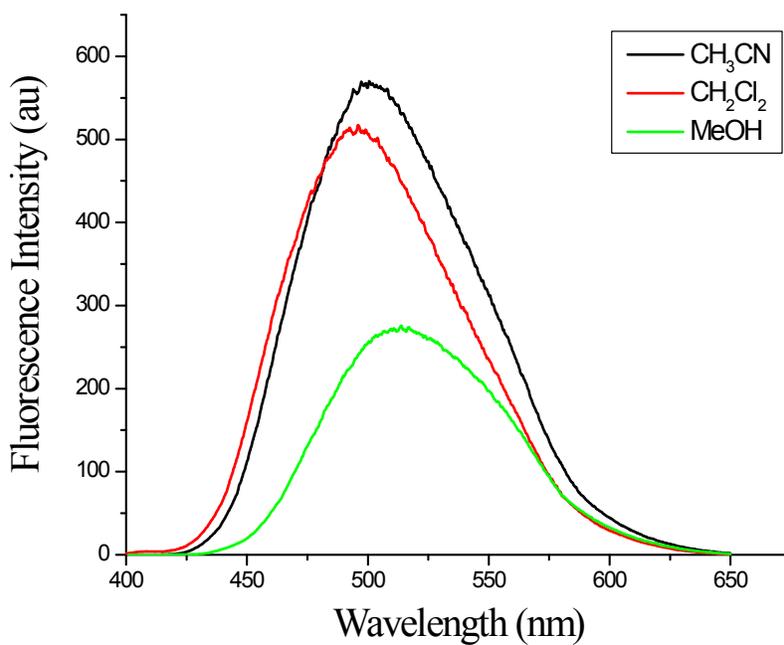
Fig. S6 Fluorescence emission spectra of **9c** in different solvents ([**9c**] = ~2×10^{-5} M).
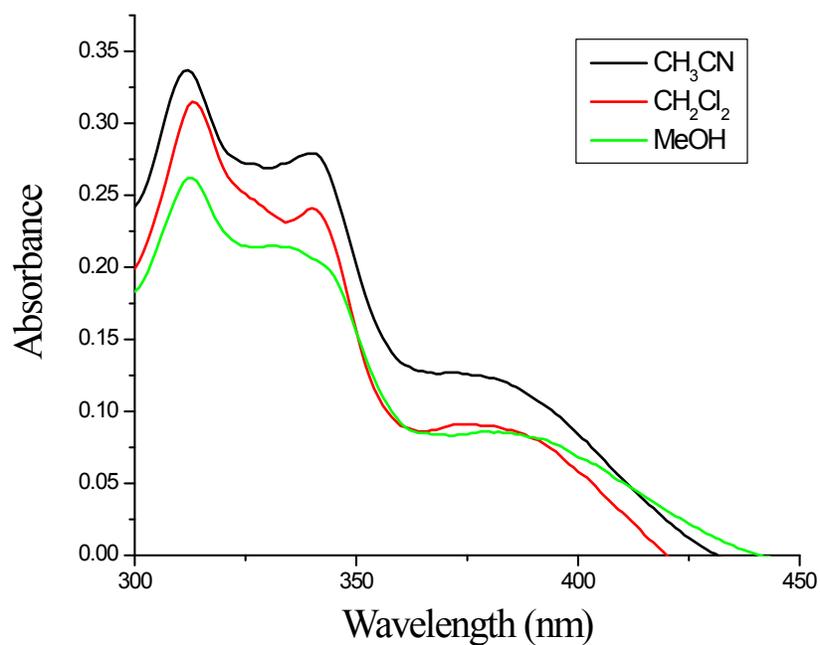
Fig. S7 UV-vis absorption spectra of compound **9e** in different solvents ([**9e**] = ~2×10^{-5} M).
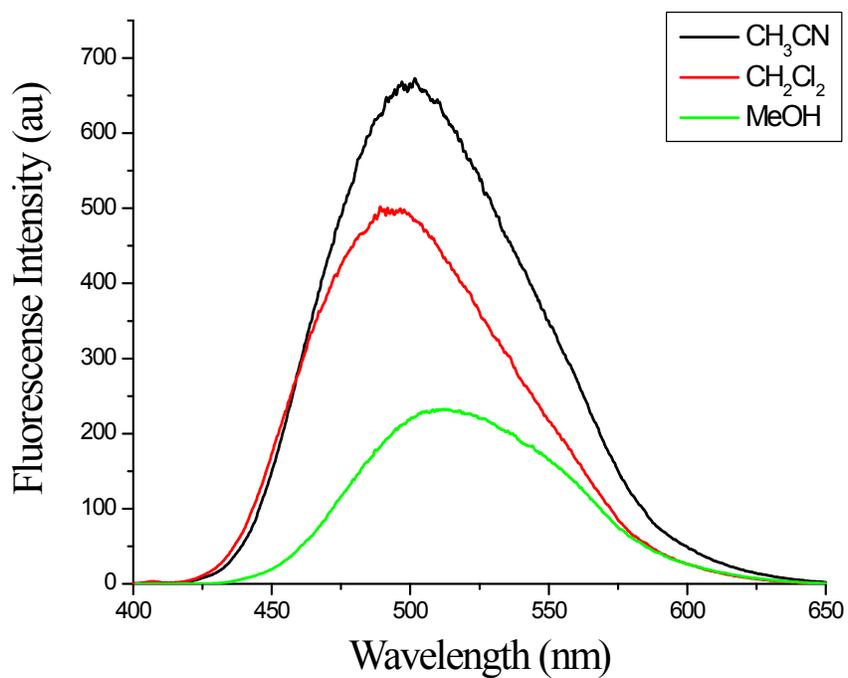
Fig. S8 Fluorescence emission spectra of **9e** in different solvents ([**9e**] = ~2×10^{-5} M).
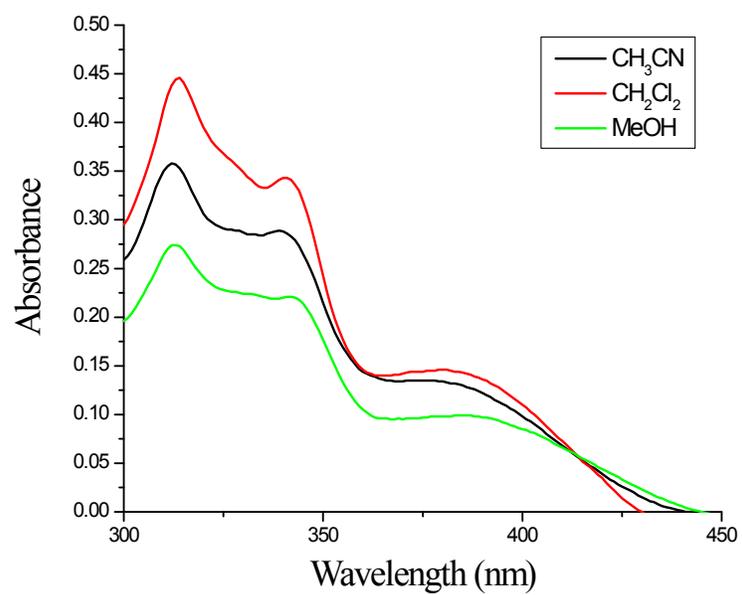
Fig. S9 UV-vis absorption spectra of compound **9f** in different solvents ([**9f**] = ~2×10^{-5} M).
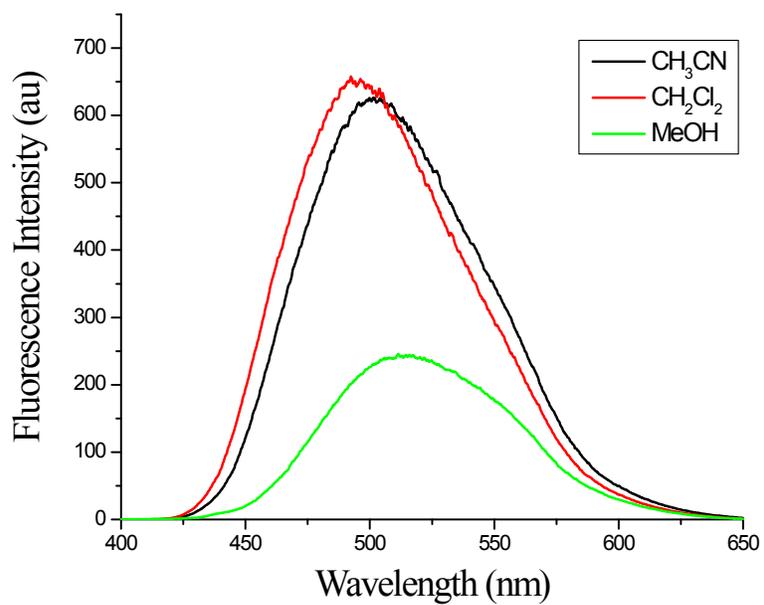
Fig. S10 Fluorescence emission spectra of **9f** in different solvents ([**9f**] = ~2×10^{-5} M).
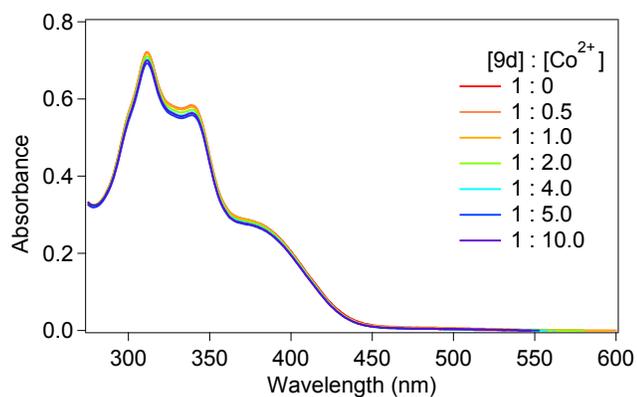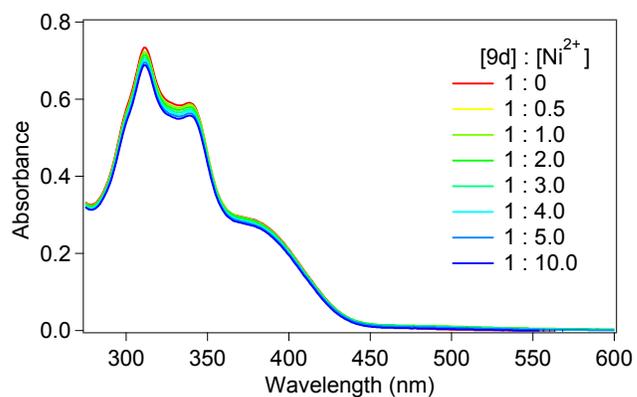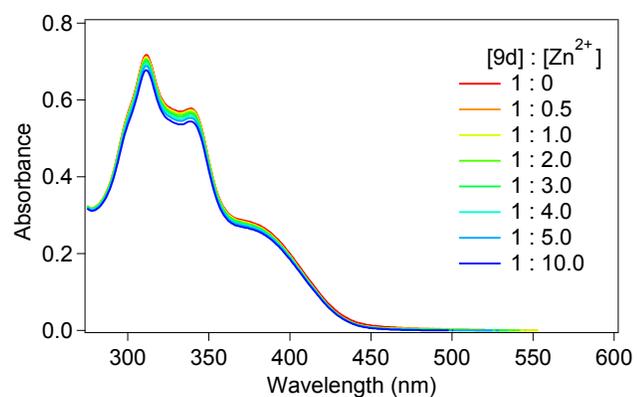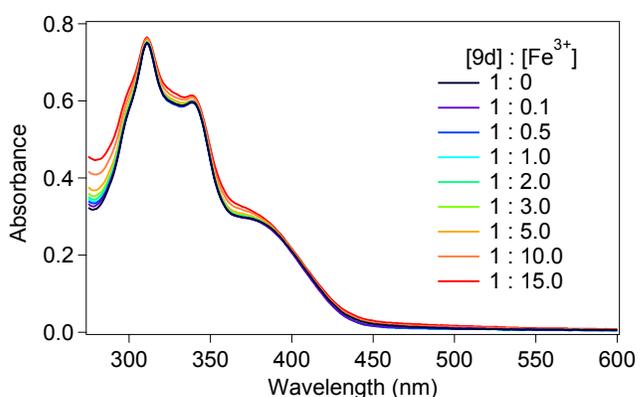
Fig. S11 Absorption spectra of **9d** in acetonitrile with increasing concentration of metal ions (a) Co^{2+}, (b) Ni^{2+}, (c) Zn^{2+} and (d) Fe^{3+}.
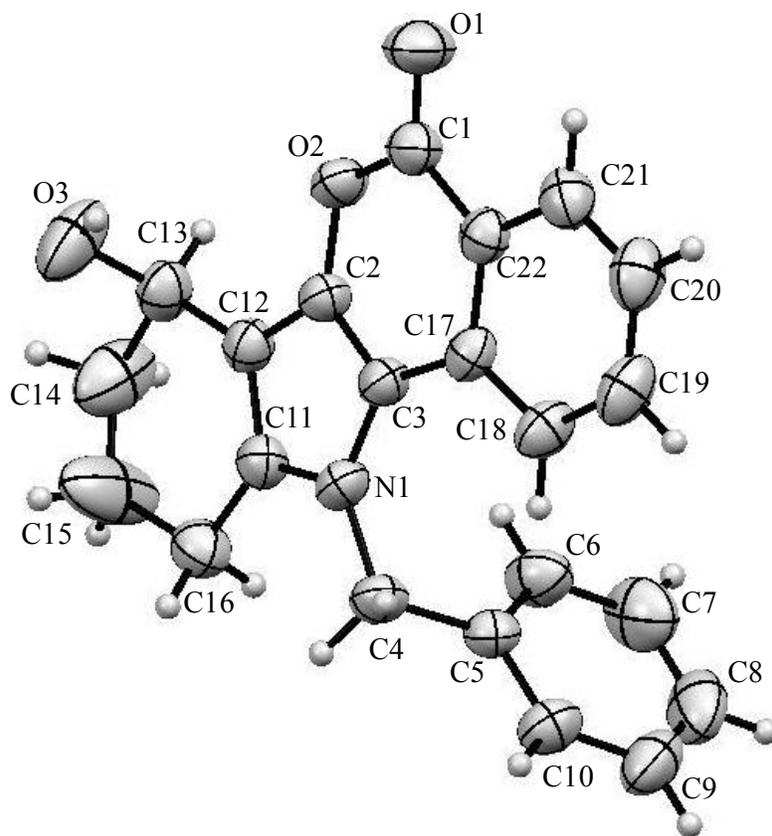
Fig. S12 ORTEP diagram of X-ray crystal structure of isocoumarin derivative **4a** where carbonyl group is reduced by $NaBH_4$ (CCDC number 940457).
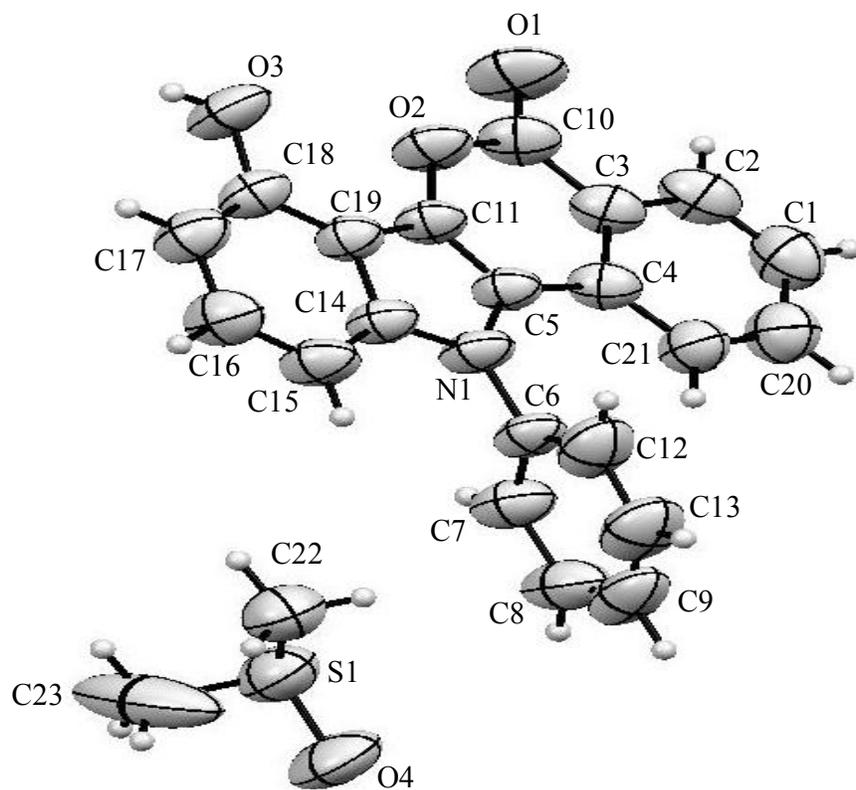
Fig. S13 ORTEP diagram of X-ray crystal structure of hydroxylindole fused isocoumarin **9b** with atom numbering scheme (CCDC number 940783).
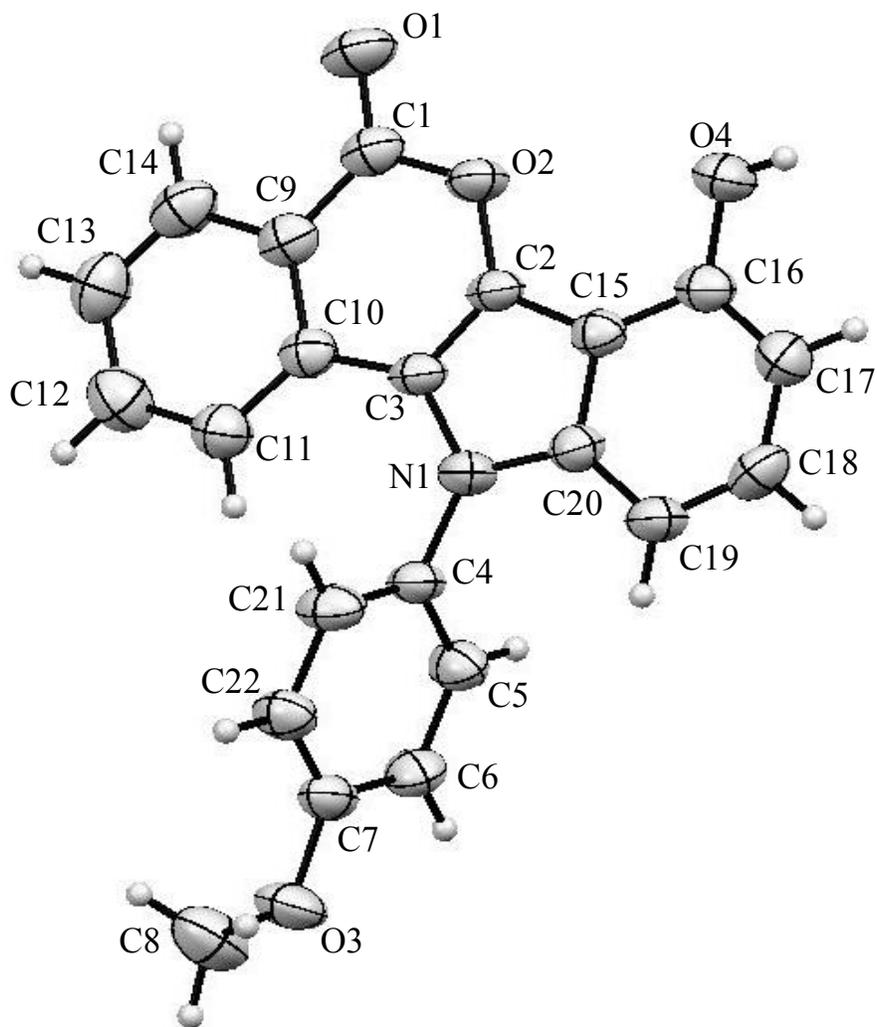
Fig. S14 ORTEP diagram of X-ray crystal structure of hydroxylindole fused isocoumarin **9f** with atom numbering scheme (CCDC number 940459).

X-ray crystal structure analyses

Crystal data

Compound 2a: $C_{22}H_{17}N_1O_3.C_6H_7N_1$, M= 436.49, monoclinic, a = 20.4475(13) Å, b = 14.4995(10) Å, c = 13.9270(9) Å, α = 90.00°, β = 106.072(2)°, γ = 90.00°, V = 3967.7(5) Å³, T = 293(2) K, space group $C2/c$, Z = 7, μ(MoKα) = 0.084 mm⁻¹, 24613 reflections measured, 4530 independent reflections ($Rint$ = 0.0387). The final $R1$ values were 0.0438 ($I > 2\sigma(I)$). The final

$wR(F2)$ values were 0.1043 ($I > 2\sigma(I)$). The final $R1$ values were 0.0761 (all data). The final $wR(F2)$ values were 0.1182 (all data). The goodness of fit on $F2$ was 1.034. CCDC number 940456.

Compound 4a: $C_{22}H_{16}N_1O_3$, M= 342.36, monoclinic, a = 13.5527(18) Å, b = 8.7440(12) Å, c = 14.7881(19) Å, α = 90.00°, β = 104.612(4)°, γ = 90.00°, V = 1695.8(4) Å^3, T = 296(2) K, space group $P2(1)/n$, Z = 4, μ(MoKα) = 0.090 mm^{-1}, 20680 reflections measured, 3875 independent reflections ($Rint$ = 0.0268). The final $R1$ values were 0.0719 ($I > 2\sigma(I)$). The final $wR(F2)$ values were 0.2021 ($I > 2\sigma(I)$). The final $R1$ values were 0.0881 (all data). The final $wR(F2)$ values were 0.2143 (all data). The goodness of fit on $F2$ was 0.975. CCDC number 940457.

Compound 9b: $C_{23}H_{19}N_1O_4S_1$, M= 405.45, Triclinic, a = 9.6997(6) Å, b = 10.1012(6) Å, c = 11.3180(12) Å, α = 96.209(3)°, β = 93.831(3)°, γ = 114.279(2)°, V = 997.31(14) Å^3, T = 296(2) K, space group $P\text{-}1$, Z = 2, μ(MoKα) = 0.192 mm^{-1}, 10955 reflections measured, 3329 independent reflections ($Rint$ = 0.0304). The final $R1$ values were 0.0949 ($I > 2\sigma(I)$). The final $wR(F2)$ values were 0.2850 ($I > 2\sigma(I)$). The final $R1$ values were 0.0949 (all data). The final $wR(F2)$ values were 0.3187 (all data). The goodness of fit on $F2$ was 1.016. CCDC number 940478.

Compound 9c: $C_{24}H_{21}NO_4S_1$, M= 419.48, triclinic, a = 9.8359(7) Å, b = 9.8990(7) Å, c = 11.8318(8) Å, α = 98.474(2)°, β = 91.399(2)°, γ = 112.007(2)°, V = 1052.42(13) Å^3, T = 296(2) K, space group $P\text{-}1$, Z = 2, μ(MoKα) = 0.184 mm^{-1}, 10390 reflections measured, 3023 independent reflections ($Rint$ = 0.0245). The final $R1$ values were 0.0783 ($I > 2\sigma(I)$). The final $wR(F2)$ values were 0.2300 ($I > 2\sigma(I)$). The final $R1$ values were 0.0900 (all data). The final $wR(F2)$ values were 0.2455 (all data). The goodness of fit on $F2$ was 1.051. CCDC number 940458.

Compound 9f: $C_{22}H_{19}N_1O_6$, M= 393.38, Triclinic, a = 9.125(8) Å, b = 10.294(8) Å, c = 10.848(9) Å, α = 87.62(4)°, β = 87.11(3)°, γ = 66.42(3)°, V = 932.5(14) Å^3, T = 296(2) K, space group *P-1*, Z = 2, μ(MoKα) = 0.103 mm^{-1}, 11248 reflections measured, 3760 independent reflections (*Rint* = 0.0656). The final *R1* values were 0.0688 ($I > 2\sigma(I)$). The final *wR(F2)* values were 0.1814 ($I > 2\sigma(I)$). The final *R1* values were 0.1250 (all data). The final *wR(F2)* values were 0.2098 (all data). The goodness of fit on *F2* was 1.041. CCDC number 940459.
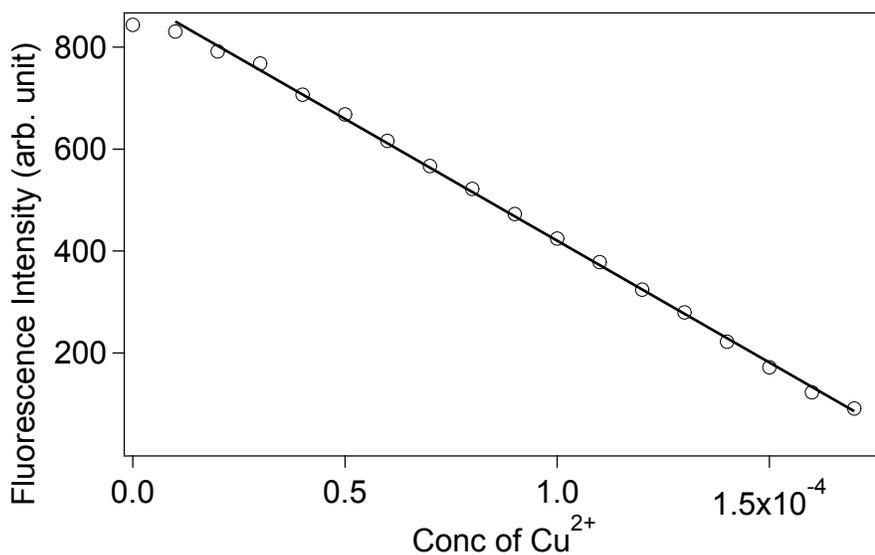
Fig. S15 Change in fluorescence intensity of **9d** in acetonitrile upon addition of Cu^{2+}

Calculation of limit of detection

The limit of detection of Cu^{2+} has been determined from fluorescence titration curves. 15-20 blank measurements (in absence of metal ion) have been measured over an extended period of time and the standard deviation corresponding to the blank measurements have been calculated. Calibration curve has been obtained by plotting fluorescence intensity against metal (Cu^{2+}) concentration. Finally the limit of detection has been calculated using the following equation

$C_L = k \times S_b / S$

C_L is the detection limit

K has been taken as 3

S_b is the standard deviation of the blank measurements

S is the slope of the calibration curve
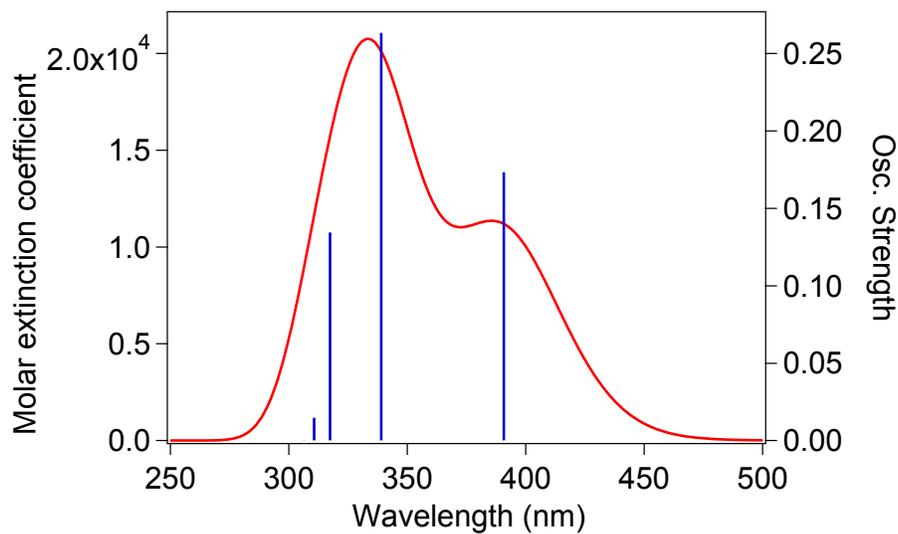
Fig. S16 Theoretically simulated UV-Vis spectra (molar exc. coefficient vs wavelength) of **9d** in methanol solvent (red curve). UV-Vis peak half width at half height = 0.22eV. The blue lines indicate the the oscillator strength for the transitions to theoretically calculated excited states.

General Information:

Starting materials and solvents were purchased from commercial suppliers and used without further purification. Melting points were determined in open capillary tubes and were uncorrected. IR spectra were recorded on a Perkin-Elmer 782 spectrophotometer. ^{1}H (300 MHz) and ^{13}C NMR (75 MHz) spectra were recorded on Bruker 300 MHz instrument in [D$_6$]DMSO. Elemental analyses (C, H and N) were performed using Perkin-Elmer 240C elemental analyzer. HRMS was performed with a QTOF I (quadrupole-hexapole-TOF) mass spectrometer. The X-ray diffraction data for crystallized compounds were collected with MoKα radiation at 296K using the Bruker APEX-II CCD System. The crystals were positioned at 50 mm from the CCD. Frames were measured with a counting time of 5s. Data analyses were carried out with the Bruker APEX2 and Bruker SAINT program. The structures were solved using direct methods with the Shelxs97 program (Sheldrick, 2008).

^{1}H NMR of **2a** in CDCl$_3$

^{13}C NMR of **2a** in CDCl$_3$

^{1}H NMR of **2b** in CDCl$_3$

^{13}C NMR of **2b** in CDCl$_3$

^{1}H NMR of **2c** in CDCl$_3$

^{13}C NMR of **2c** in CDCl$_3$

^{1}H NMR of **2d** in CDCl$_3$

^{13}C NMR of **2d** in CDCl$_3$

^{1}H NMR of **2e** in CDCl$_3$

^{13}C NMR of **2e** in CDCl$_3$

^{1}H NMR of **2f** in CDCl$_3$

^{13}C NMR of **2f** in CDCl$_3$

^{1}H NMR of **2g** in CDCl$_3$

^{13}C NMR of **2g** in CDCl$_3$

^{1}HNMR of **2h** in CDCl$_3$

^{13}CNMR of **2h** in CDCl$_3$

^{1}H NMR of **2i** in CDCl$_3$

^{13}C NMR of **2i** in CDCl$_3$

^{1}H NMR of **2j** in CDCl$_3$

^{13}C NMR of **2j** in CDCl$_3$

^{1}H NMR of **2k** in CDCl$_3$

^{1}H NMR of **3a** in CDCl$_3$

^{13}C NMR of **3a** in CDCl$_3$

^{1}H NMR of **3b** in CDCl$_3$

^{13}C NMR of **3b** in CDCl$_3$

^{1}H NMR of **3c** in CDCl$_3$

^{13}C NMR of **3c** in CDCl$_3$

^{1}H NMR of **3d** in CDCl$_3$

^{13}C NMR of **3d** in CDCl$_3$

^{1}H NMR of **3e** in CDCl$_3$

^{13}C NMR of **3e** in CDCl$_3$

^{13}C NMR of **3f** in CDCl$_3$

^{13}C NMR of **3f** in CDCl$_3$

^{1}H NMR of **3g** in CDCl$_3$

^{13}C NMR of **3g** in CDCl$_3$

^{1}H NMR of **3h** in CDCl$_3$

^{13}C NMR of **3h** in CDCl$_3$

^{1}H NMR of **3i** in CDCl$_3$

^{13}C NMR of **3i** in CDCl$_3$

^{1}H NMR of **3j** in CDCl$_3$

^{13}C NMR of **3j** in CDCl$_3$

^{1}H NMR of **3k** in CDCl$_3$

^{13}C NMR of **3k** in CDCl$_3$

^{1}H NMR of **9a** in d$_6$-DMSO

^{1}H NMR of **9a** in d$_6$-DMSO

^{13}C NMR of **9a** in d$_6$-DMSO

HRMS of **9a**

^{1}H NMR of **9b** in d$_6$-DMSO

^{13}C NMR of **9b** in d$_6$-DMSO

HRMS of **9b**

^{1}H NMR of **9c** in d$_6$-DMSO

^{13}C NMR of **9c** in d$_6$-DMSO

HRMS of **9c**

^{1}H NMR of **9d** in d$_6$-DMSO

^{13}C NMR of **9d** in d$_6$-DMSO

^{1}H NMR of **9e** in d$_6$-DMSO

^{13}C NMR of **9e** in d$_6$-DMSO

^{1}H NMR of **9f** in d$_6$-DMSO

^{13}C NMR of **9f** in d$_6$-DMSO

HRMS of **9f**

^{1}H NMR of **4a** in CDCl$_3$

^{13}C NMR of **4a** in CDCl$_3$

^{1}H NMR of **4b** in CDCl$_3$

^{13}C NMR of **4b** in CDCl$_3$